Journal of the Brazilian Society of Mechanical Sciences and Engineering (2020) 42:562
https://doi.org/10.1007/s40430-020-02613-x

TECHNICAL PAPER

# Soft computing method for predicting pressure drop reduction in crude oil pipelines based on machine learning methods

**Hossein Moayedi[1,2] · Loke Kok Foong[3,4] · Hoang Nguyen[5]**

Received: 30 March 2019 / Accepted: 3 September 2020


## Abstract

In the oil industry, the drag-reducing agent has been used to reduce turbulent friction of fluids. The main effort of this study is to examine the feasibility of four novel machine learning models, namely multilayer perceptron, M5Rules, decision table (DT), and trees M5P to estimate the percentage of drag reduction. Then, the mentioned methods are utilized to identify a relationship between the input and output parameters of the crude oil pipeline system. The parameter percentage of drag reduction was taken as the essential output. In contrast, the input parameters selected the flow rate of oil, polymer concentration, kind of polymer, temperature, as well as pipe diameter and roughness. The predicted results obtained by the tools mentioned above were evaluated according to several known statistical indices, namely coefficient of determination ($R^2$), mean absolute error (MAE), root mean squared error (RMSE), relative absolute error (RAE), and root relative squared error (RRSE) as well as novel ranking systems of color intensity rating and total ranking method. The training and testing results of the DT learning method for the $R^2$, MAE, RMSE, RAE, and RRSE were (0.9616, 3.9008, 5.8698, 24.5259%, and 27.4406%) and (0.8964, 6.937, 10.318, 43.3841%, and 45.6581%), respectively. The obtained results, in analyzing the training and testing datasets, proved that DT is the best predictive network to predict the percentage of drag reduction.

**Keywords** Crude oil · Drag-reducing agent · Pressure drop · Multilayer perceptron · M5 rules · Decision table · Trees M5P

## 1 Introduction

Turbulence can be described as a fluctuating and chaotic fluid motion, which manifests when nonlinear inertia effects dominate over viscous effects [1]. In other words, most operating systems require pumping fluids at high flow rates, which, in turn, generates high frictional pressure losses. By reducing the turbulence of the flow, drag-reducing agents can reduce the energy consumption of pumping. A spectacular reduction in energy losses in turbulent flows can be achieved by the addition of small amounts of specific polymers. Drag-reducing agent (DRA) has been employed widely in the oil industry, to reduce the rate of turbulent friction of fluids [2]. Polymer drag reduction is due to the large elongational viscosity of the polymer solution; this stabilizes the turbulent boundary layer, leading to a decrease in the pressure drop in turbulent flows [3]. Drag-reducing polymer solution flows behave like viscoelastic characteristics. The most notable elastic property of the viscoelastic polymer solution is that stress does not immediately become zero when the fluid motion stops, but rather decays with appropriate time (i.e., the relaxation time), which can reach seconds

Technical Editor: Celso Kazuyuki Morooka.

**Electronic supplementary material** The online version of this article (https://doi.org/10.1007/s40430-020-02613-x) contains supplementary material, which is available to authorized users.

✉ Loke Kok Foong
lokekokfoong@tdtu.edu.vn

Hossein Moayedi
hosseinmoayedi@duytan.edu.vn

[1] Institute of Research and Development, Duy Tan University, Da Nang 550000, Vietnam

[2] Faculty of Civil Engineering, Duy Tan University, Da Nang 550000, Vietnam

[3] Department for Management of Science and Technology Development, Ton Duc Thang University, Ho Chi Minh City, Vietnam

[4] Faculty of Civil Engineering, Ton Duc Thang University, Ho Chi Minh City, Vietnam

[5] Hanoi University of Mining Land Geology, 18 Vien Street, Duc Thang Ward, Bac Tu Liem District, Hanoi, Vietnam

Published online: 08 October 2020

and even minutes. It is generally believed that the frictional drag reduction caused by polymer and surfactant additives in a wall-bounded flow is the consequence of the interaction between viscoelasticity and turbulence in the flow [4]. This network microstructure imparts viscoelasticity to the solution flow, which was often stated to be responsible for the occurrence of drag reduction [5, 6]. Primary studies were conducted by Toms [7] and Mysels [8] on drag reduction. They investigated the effect of adding some polymers for reducing skin friction and pressure drop in pipelines in their individual studies. The experimental work done by Toms [7] led to the drag reduction effect being known as Toms' effect. Due to the vital importance of this subject, numerous studies have focused on various parameters affecting drag reduction. Among these works, some of them are considerable [9–15].

Accurate determination of the friction pressure losses of dilute drag-reducing polymer solutions has remained a challenge in many practical applications. A polymer solution, even in a very dilute form, can be regarded as a viscoelastic fluid. In fact, due to the ability of polymers to store elastic energy, elasticity can propagate shear waves. These shear waves provide a natural cutoff that fluctuates at high frequencies. Then, the cutoff would suppress the small eddies and, presumably, lead to drag reduction. Several researchers conducted a comprehensive study on drag reduction for water flow and proposed relationships for the Fanning friction factor, which helps other researchers to analyze their results [16–19]. Virk [20] investigated the performance of different polymer solutions and found a trend to a maximum drag reduction (MDR) asymptote in all cases. Sher and Hetsroni [21] proposed a mechanistic model for the turbulent drag reduction by additives, in accordance with the elastic properties of polymer, and compared their results with other studies [22, 23].

Due to the importance of this subject, numerous studies have focused on different operating parameters affecting drag reduction. In this regard, various researchers [24–27] investigated the effect of pipe diameter on drag reduction and found that the drag reduction percentage increases by decreasing the pipe diameter. The impact of relative roughness of pipe on DR% was also investigated by Mowla and Naderi [25]. They proved that the higher DR% could be obtained at rougher pipes. Another parameter with significant effects on drag reduction is the concentration of DRA. They proposed a mathematical model for predicting the drag reduction by a given polymer at two-phase flow. Their proposed model could also be used for calculating friction and maximum drag reduction as a function of DRA concentration. Gallego and Shah [28] developed a generalized friction pressure correlation for the phenomenon in coiled and straight tubing on the basis of the energy dissipation of eddies in turbulent flow fields and shear rate dependent relaxation time. They found that their model in straight tubing correlated better than the previously developed models. Also, Shah et al. [29] developed new correlations for predicting the friction factor values as a function of the solvent's Reynolds number for both straight and coiled tubing using the data of an optimum concentration of the polymeric fluid. Most recently developed prediction techniques employed the computer science advances and intended to find a reliable solution in solving engineering and medical related problems. In this sense, the technique of extreme machine learning approaches [30–32, 33], Harris hawks optimization [34, 35], spatial adjacent histogram [36], fruit fly optimization [37], chaotic moth-flame optimization [38, 39, 40], multi-swarm whale optimizer [41], grey wolf optimization [42] can be mentioned. Such multi-disciplinary techniques are widely used as analysis tools in most complex engineering projects such as building information modelling [43, 44], sustainable sediment management in hydropower [45], contractors' dynamic price competition in mega projects [46], emotion recognition and image sharing [47], wireless sensor networks [48, 49], big data application [50, 51], landslide prediction over a large region [52], Digital Neuromorphic Architecture [53].

Due to the significance of the issue, the present study involves proposing a mathematical model for relating the drag reduction (PDR) with various parameters. Also, the effect of additives concentration, pipe diameter, solution flow rate, and the presence of radius elbows on the percentage of drag reduction (%DR) and the number of flow increases (%FI) were the variables of the study. The primary purpose of the present investigation was to make a reliable machine learning to calculate pressure drop reduction of crude oil pipelines. Firstly, four different machine learning-based solutions were selected including multilayer perceptron (MLP), M5Rules (M5R), decision table (DT), and trees M5P (TM5P). Then, the obtained results of predictions are analyzed and discussed.

## 2 Materials and methods

### 2.1 Artificial intelligence-based solution

The data-driven statistical concepts and machine learning-based techniques that have been employed to estimate the percentage of drag reduction are briefly described in this section.

#### 2.1.1 Multilayer perceptron (MLP)

Multilayer perceptron (MLP) is one of the most common types of artificial neural networks (ANN). Inspired by the biological neural network, ANN was first presented in 1949 [54]. A prominent superiority of ANN is the ability of nonlinear mapping over a dataset (i.e., inputs and the

corresponding targets) [55]. Due to this merit, many scholars have successfully developed the MLP neural network in various fields of study [56–59, 53, 60]. In general, two types of data are required for implementing an ANN. The major part of the dataset is specified for training the network (training data), and the quality of this process is evaluated by using the testing data. The training procedure is usually carried out by the "back propagation" (BP) method [61–63]. In this sense, the main effort of BP is to minimize the error performance (i.e., the difference between the actual and estimated outputs) through propagating on a backward path. The ANN parameters are adjusted in each iteration to produce a more compatible output vector. In addition to the network structure, the number of epochs, activation function, and learning law is three factors that influence the performance of ANN [64]. The proposed MLP structure in this study was used with a single hidden layer having six nodes.

#### 2.1.2 M5Rules

Similar to many other machine learning methods, tree learning (TL) is the essence of the M5Rules model. A straightforward working method that extracts rules from model trees is known as M5Rules. This model has been employed for various classification and prediction issues [65]. M5Rules uses a tree learner over the training samples to train a pruned tree. Then, the elite leaf is made into a rule, and the tree is discarded. Note that, this action can be mentioned as the sole difference between M5rules and regular process that creates a single rule. In the following, all samples covered by the specific rule are eliminated from the records. This procedure stops when entire instances are covered by at least one rule. Achieving the rules from the best leaf leads to decreases risk of over-pruning. Unlike the partial decision trees (PART), which generates partially explored trees, M5Rules produces full trees. Generating partial trees causes not only a higher level of computational veracity but also has no impact on the size and accuracy of the obtained rules [66]. For the proposed M5Rules, the batch size = 100, minimum number of instances were 4, number of decimal places = 2. Other terms such as build regression tree, debug, save instances, unpruned, and use unsmoothed conditions were set to be false.

### 2.2 Decision table (DT)

Decision table (DT) sorts the rules and classes in some rows and columns (i.e., tabular form). Given a new instance, DT aims to find an exact match in the table. Accordingly, two responses are possible: if the desired match is found, it will be considered as the answer. Otherwise, the system announces no match is found [67]. Up to now, DT has been effectively employed in various fields [68, 69]. Also, Abbinaya and Kumar [70] trained a DT by neural networks for software effort estimations. Due to its straightforward architecture, DT is a more stable and suitable method compared to the decision tree technique, which has a hierarchical structure. Generally, a DT composed of four sections: condition stubs, condition entries, action stubs, and action entries. In this regard, action rules, required actions, condition rules (or alternatives), and conditions lie in the lower right quadrature, lower left quadrature, upper right quadrature, and upper left quadrature, respectively. The validation stage is easy for DT to check cases such as incompleteness and contradiction [71]. For the proposed DT method, the batch size was considered to be 100, the cross validation was equal to 1 and number of decimal places considered to be 2. In this sense, the other terms such as debug, display rules, and using IBK were set to be false.

#### 2.2.1 Trees M5P (TM5P)

The name M5P tree (M5P) indicates an enhanced version of Quinlan's M5 technique for regression works [72]. As a regression classifier, it uses a straightforward criterion. In this model, a conventional decision tree is combined with the possibility of linear regression at the leaves. Firstly, a tree is built by employing a decision tree. Note that, a splitting criterion is performed at every inner node instead of maximizing the gained information. The main task of this criterion is to minimize the intra-subset variation in the level of water at each branch. One of the stopping conditions of the performing splitting nodes is the slight variation of the level of water of all samples. Pruning the developed tree is the second, that during this process, an inner node exchanges a leaf with a regression aim. Finally, a smoothing process is applied to synthesize leaf method prediction with each node. Notably, this process occurs along the route back to the root [73]. In this study, meta-parameters used in M5Rules training process was used for the proposed M5P technique.

### 2.3 Database collection

In order to propose a general model involving oil flow rate and temperature, pipe diameter, and roughness and the type of DRA and concentration, an experimental apparatus, as shown in Fig. 1, was constructed to carry out the experiments.

Various concentrations of three types of dilute polymeric solutions as drag-reducing agents have been tested at four temperatures and flow rates in the apparatus installed with three pipes, each with a different value for diameter and roughness. Pipe no. 1 is 1 inch in diameter, a rough pipe of galvanized iron (relative roughness); pipe no. 2 is 1 inch in diameter, a smoother pipe of carbon steel and pipe no. 3 is 0.5 inch in diameter of the galvanized iron. All pipes were

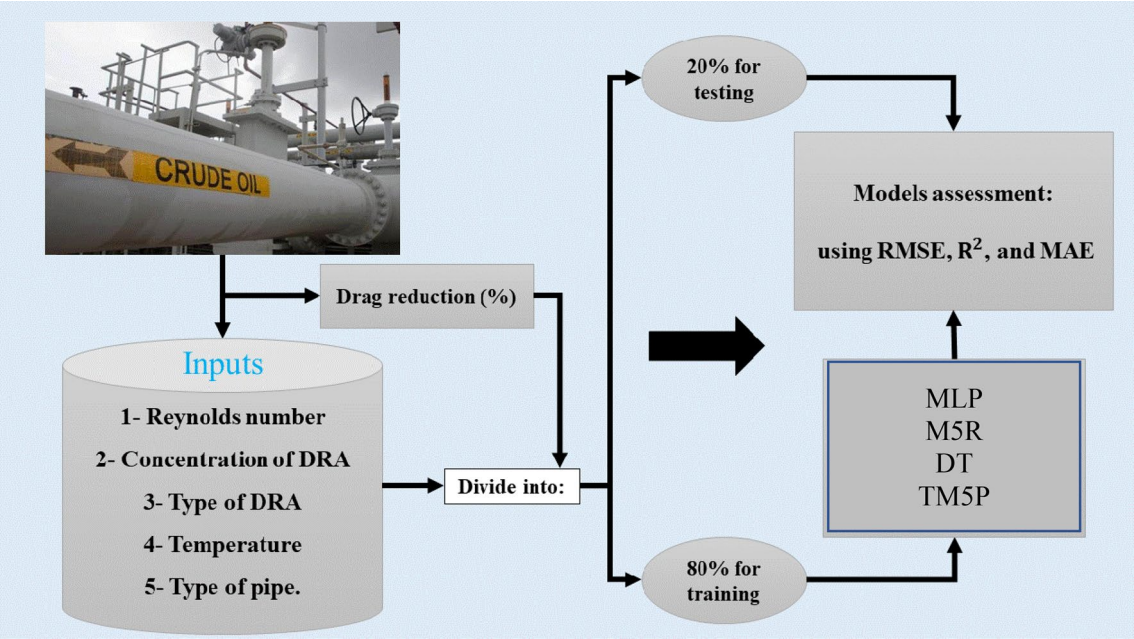


**Fig. 1** Graphical methodology of applied procedure for DR modeling

8.8 m long. A progressive pump has done the circulation of the fluid through each pipe. Flow rates of the circulating crude oil are measured by a rotameter. Pressure drop is measured between two points with a distance of 5.6 m. The parameter percentage of drag reduction (PDR) was taken as the essential output, while the input parameters selected the Reynolds number, polymer concentration, type of polymer, temperature as well as pipe numbers. Changes in temperature are induced by a shell and tube heat exchanger that cools the fluid entering the pump. Heating is achieved using a heating element placed inside the crude oil tank. A thermometer is also placed at the entrance of the pipes to measure the temperature. The compositions of these polymers include: DRA1 [polyolefin synthetic rubber (33 wt%), polyethylene wax (12%), polyacrylic acid (1%), aluminum particle (5%), and propylene glycol (49%)] DRA2 [ethylene–propylene–copolymer (33 wt%), polyethylene wax (12%), polyacrylic acid (1%), and propylene glycol (54%)] DRA3 [polypropylene (48%), ethylene glycol (39%), surfactant (8%), water (3%), and polyacrylic acid (2%)]. The physical properties of crude oil provided by the Shiraz oil refinery were calculated according to ASTM D-445 and ASTM D 1217-81.

All the experiments have been run at four different temperatures of 4, 15, 29, and 41 °C. To investigate the effect of various DRAs on pressure drop reduction of crude oil, three types of polymeric DRAs are used in this study. In each experiment, a given amount of the employed DRA is added to the crude oil, and changes in pressure drop are measured. Since the ranges of the concentrations of added DRA made no observable change in the properties of the crude oil, the rheological properties of the fluid remain constant. Thus, in this work, 348 instances, including five input factors of Reynolds number, concentration, and type of drag-reducing agents, temperature, and type of pipe and drag reduction as the response parameter, construct the mentioned dataset. The database used to make machine learning models were obtained from previous studies that reviewed the percentage of drag reduction [2, 24, 74]. The following equations were used to calculate Reynolds number (Re), percentage drag reduction (DR%), respectively:

$$\mathrm{Re} = \frac{\rho v d}{\mu} \tag{1}$$

$$\mathrm{DR}\% = \frac{|\Delta p_1 - \Delta p_2|}{\Delta p_1} \times 100 \tag{2}$$

where $\rho$ is density, $v$ liner velocity, $d$ pipe diameter, $\mu$ viscosity, $\Delta P_1$ $\Delta P_2$ pressure drop before and after the addition of polymer and $L$ is pipe length. Table 1. An example of data samples used for predicting response.

The graphical description of these parameters is illustrated in Fig. 2a–f showing the data number versus the Reynolds number, polymer concentration, kind of polymer, temperature, and pipe numbers.

**Table 1** An example of data samples used for predicting the percentage of drag reduction

| No. | Input | | | | | Output |
|---|---|---|---|---|---|---|
| | Reynolds number (N/A) | Polymer concentration (mg/l) | Kind of polymer (N/A) | Temperature (°C) | Pipe numbers (N/A) | Percentage of drag reduction (%) |
| 1 | 6104.84 | 25 | 1 | 29 | 1 | 3.15 |
| 2 | 9940.11 | 25 | 1 | 29 | 1 | 4.21 |
| 3 | 13,531.89 | 25 | 1 | 29 | 1 | 4.98 |
| 4 | 16,777.77 | 25 | 1 | 29 | 1 | 5.95 |
| 5 | 6104.84 | 50 | 1 | 29 | 1 | 3.81 |
| 6 | 9940.11 | 50 | 1 | 29 | 1 | 5.04 |
| 7 | 13,531.89 | 50 | 1 | 29 | 1 | 7.08 |
| 8 | 16,777.77 | 50 | 1 | 29 | 1 | 9.77 |
| 9 | 6104.84 | 75 | 1 | 29 | 1 | 6.76 |
| 10 | 9940.11 | 75 | 1 | 29 | 1 | 9.04 |
| 11 | 13,531.89 | 75 | 1 | 29 | 1 | 11.98 |
| 12 | 16,777.77 | 75 | 1 | 29 | 1 | 14.92 |
| 13 | 6104.84 | 100 | 1 | 29 | 1 | 14.83 |
| 14 | 9940.11 | 100 | 1 | 29 | 1 | 19.01 |
| 15 | 13,531.89 | 100 | 1 | 29 | 1 | 21.8 |
| 16 | 16,777.77 | 100 | 1 | 29 | 1 | 25.17 |
| 17 | 6104.84 | 150 | 1 | 29 | 1 | 24.87 |
| 18 | 9940.11 | 150 | 1 | 29 | 1 | 31.53 |
| 19 | 13,531.89 | 150 | 1 | 29 | 1 | 34.02 |
| 20 | 16,777.77 | 150 | 1 | 29 | 1 | 38.65 |
| 21 | 6104.84 | 200 | 1 | 29 | 1 | 27.29 |
| 22 | 9940.11 | 200 | 1 | 29 | 1 | 34.67 |
| 23 | 13,531.89 | 200 | 1 | 29 | 1 | 38.22 |
| 24 | 16,777.77 | 200 | 1 | 29 | 1 | 44.06 |
| 25 | 2192.05298 | 150 | 1 | 4 | 1 | 14.67352 |
| 26 | 4019.86755 | 150 | 1 | 4 | 1 | 18.82094 |
| 27 | 5695.364238 | 150 | 1 | 4 | 1 | 21.00148 |
| 28 | 7294.701987 | 150 | 1 | 4 | 1 | 24.66126 |
| 29 | 4248.344371 | 150 | 1 | 15 | 1 | 23.00262 |
| 30 | 7370.860927 | 150 | 1 | 15 | 1 | 30.81635 |

## 2.4 Model validation and accuracy

The training process was performed entirely in WEKA software, which is a useful framework for data mining and classification. Note that, many researchers have employed WEKA formerly for various simulating aims. Five statistical indices, including $R^2$, MAE, RMSE, RAE, and RRSE were used to develop a colour intensity ranking to present a colored comparison of the results. This can be noted that these criteria have been extensively used in earlier studies. Equations (3) to (7) describe the formulation of $R^2$, MAE, RMSE, RAE, and RRSE, respectively.

$$R^2 = 1 - \frac{\sum_{i=1}^{s}(Y_{i_{\text{predicted}}} - Y_{i_{\text{observed}}})^2}{\sum_{i=1}^{s}(Y_{i_{\text{observed}}} - \bar{Y}_{\text{observed}})^2} \tag{3}$$

$$\text{MAE} = \frac{1}{N}\sum_{I=1}^{s}\left|Y_{i_{\text{observed}}} - Y_{i_{\text{predicted}}}\right| \tag{4}$$

$$\text{RMSE} = \sqrt{\frac{1}{N}\sum_{i=1}^{s}\left[\left(Y_{i_{\text{observed}}} - Y_{i_{\text{predicted}}}\right)\right]^2} \tag{5}$$

$$\text{RAE} = \frac{\sum_{i=1}^{s}\left|Y_{i_{\text{predicted}}} - Y_{i_{\text{observed}}}\right|}{\sum_{i=1}^{s}\left|Y_{i_{\text{observed}}} - \bar{Y}_{\text{observed}}\right|} \tag{6}$$

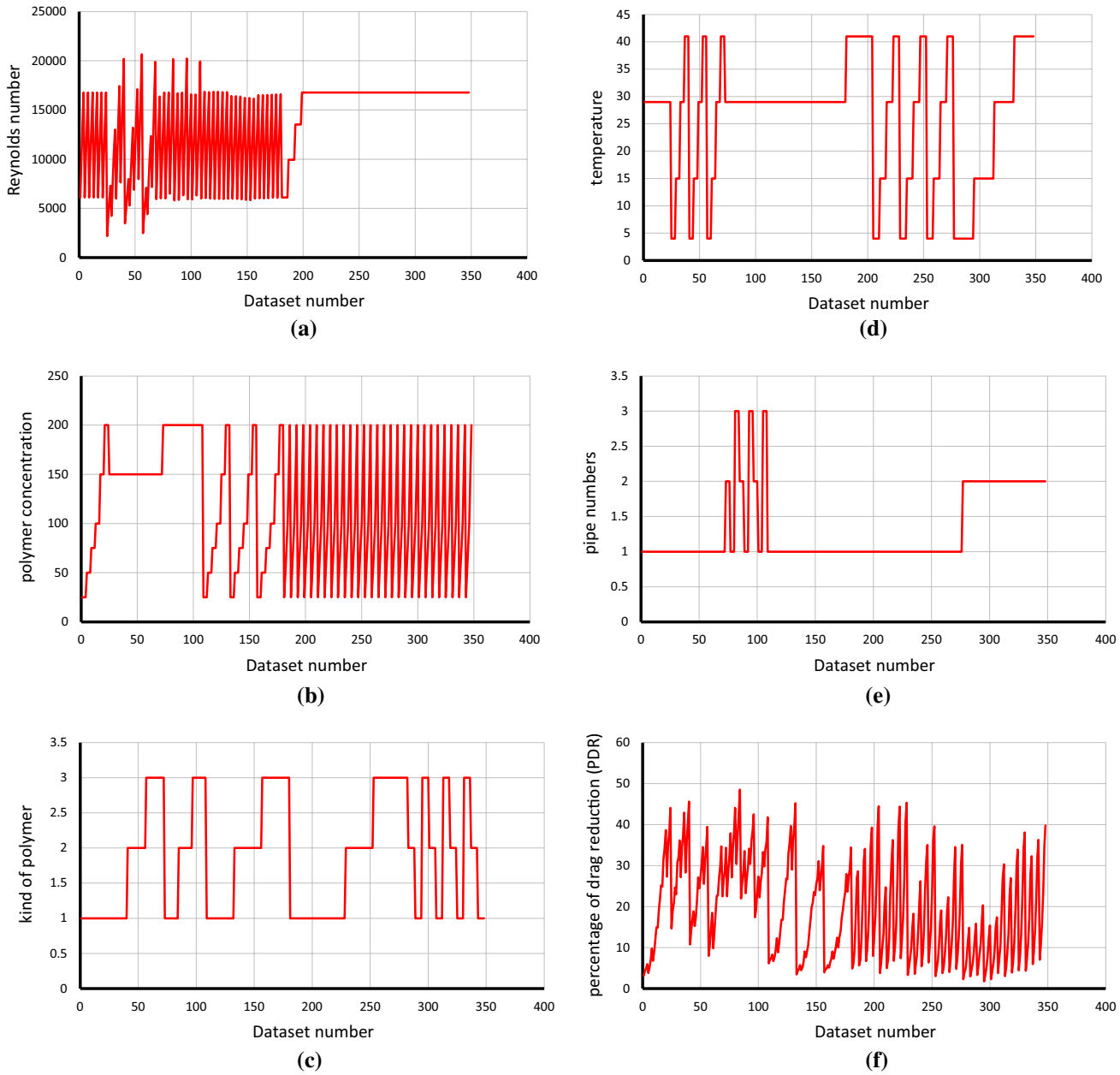


**Fig. 2** Graphical description of the range of input data versus data numbers for **a** Reynolds number, **b** polymer concentration, **c** kind of polymer, **d** temperature, **e** pipe numbers, and **f** actual PDR

$$\mathrm{RRSE} = \sqrt{\frac{\sum_{i=1}^{s}(Y_{i_{\mathrm{predicted}}} - Y_{i_{\mathrm{observed}}})^2}{\sum_{i=1}^{s}(Y_{i_{\mathrm{observed}}} - \bar{Y}_{\mathrm{observed}})^2}} \tag{7}$$

wherein all the above equations, $Y_{i\ \mathrm{observed}}$, and $Y_{i\ \mathrm{predicted}}$ we denote the actual and predicted values of response, respectively. The term S represents the number of data, and $\bar{Y}_{\mathrm{observed}}$ stands for the average of the actual values of the percentage of drag reduction. In the next part of this paper, the accuracy of applied models (i.e., MLP, M5R, DT, and TM5P) for the approximation of response is presented and discussed.

## 3 Results and discussion

The main concentration of this research is to appraise the competency of four standard machine learning tools, namely MLP, M5R, DT, and TM5P, in estimating the percentage

of drag reduction. For this aim, as mentioned before, five input factors of Reynolds number, concentration, and type of drag reducing agents, temperature, and type of pipe were selected. The input database is provided from the previous literature study. To create the required training data samples, the critical parameters were listed against the corresponding responses. In this regard, 80% of the gathered dataset was randomly selected for training the models MLP, M5R, DT, and TM5P (training phase comprising 278 samples). Then, the competency of each model was evaluated using the remaining 20% of the dataset (testing phase containing 70 samples).

## 4 Model assessment in the percentage of drag reduction prediction

The calculated values of $R^2$, MAE, RMSE, RAE, and RRSE for estimating the response are tabulated in Tables 2 and 3 for training and testing datasets. Also, the total ranking obtained for models is featured in Table 4. The same process is provided in other machine learning-based studies (e.g., [30–33], [36–39], [41], [42], [75], [76]). A graphical exhibition of the results is also presented, based on a colour intensity model. A red collection is considered for these tables. In this sense, a higher value of $R^2$ and less MAE, RMSE, RAE, and RRSE have been addressed by a more intense red color. The final ranking was determined concerning the total score obtained for MLP, M5R, DT, and TM5P models. This is noteworthy that the proposed total score indicates the summation of the partial scores given based on the $R^2$, MAE, RMSE, RAE, and RRSE for each model (see Tables 2, 3, 4).

The results of statistical indexes ($R^2$, MAE, RMSE, RAE, and RRSE) for the training datasets in MLP, M5R, DT, and TM5P were (0.9122, 10.1273, 11.6416, 63.6743%, and 54.4225%), (0.9032, 6.4502, 9.2499, 40.5548%, and 43.242%), (0.9616, 3.9008, 5.8698, 24.5259%, and 27.4406%), and (0.8851, 7.1503, 10.1877, 44.9566%, and 47.6261%), respectively (Table 2). Similarly, for the testing datasets, the $R^2$, MAE, RMSE, RAE, and RRSE of in MLP, M5R, DT, and TM5P datasets were (0.8109, 8.5967, 13.7492, 53.7642, and 60.8413), (0.9025, 7.5829, 9.983, 47.4238, and 44.1757), (0.8964, 6.937, 10.318, 43.3841, and 45.6581), and (0.8671, 8.8394, 11.831, 55.282, and 52.3533), respectively (Table 3). In a glance, after reviewing both training and testing datasets, it can be seen that the DT technique can be introduced as the outstanding model, due to the highest total and partial scores obtained for it. M5R predictive model presents the most effective training compared to other models. Also, DT can be introduced as the second accurate models, respectively. Furthermore, it

**Table 2** The results of proposed networks based on several statistical indexes (provided for training dataset only)

| | Proposed models | Network results | | | | | Ranking the predicted models | | | | | Total ranking score | Rank |
|---|---|---|---|---|---|---|---|---|---|---|---|---|---|
| | | $R^2$ | MAE | RMSE | RAE (%) | RRSE (%) | $R^2$ | MAE | RMSE | RAE (%) | RRSE (%) | | |
| 1 | MLP | 0.9122 | 10.1273 | 11.6416 | 63.6743 | 54.4225 | 3 | 1 | 1 | 1 | 1 | 7 | 4 |
| 2 | M5R | 0.9032 | 6.4502 | 9.2499 | 40.5548 | 43.242 | 2 | 3 | 3 | 3 | 3 | 14 | 2 |
| 3 | DT | 0.9616 | 3.9008 | 5.8698 | 24.5259 | 27.4406 | 4 | 4 | 4 | 4 | 4 | 20 | 1 |
| 4 | TM5P | 0.8851 | 7.1503 | 10.1877 | 44.9566 | 47.6261 | 1 | 2 | 2 | 2 | 2 | 9 | 3 |

**Table 3** The results of proposed networks based on several statistical indexes (provided for testing dataset only)

| | Proposed models | Network results | | | | | Ranking the predicted models | | | | | Total ranking score | Rank |
|---|---|---|---|---|---|---|---|---|---|---|---|---|---|
| | | $R^2$ | MAE | RMSE | RAE (%) | RRSE (%) | $R^2$ | MAE | RMSE | RAE (%) | RRSE (%) | | |
| 1 | MLP | 0.8109 | 8.5967 | 13.7492 | 53.7642 | 60.8413 | 1 | 2 | 1 | 2 | 1 | 7 | 4 |
| 2 | M5R | 0.9025 | 7.5829 | 9.983 | 47.4238 | 44.1757 | 4 | 3 | 4 | 3 | 4 | 18 | 1 |
| 3 | DT | 0.8964 | 6.937 | 10.318 | 43.3841 | 45.6581 | 3 | 4 | 3 | 4 | 3 | 17 | 2 |
| 4 | TM5P | 0.8671 | 8.8394 | 11.831 | 55.282 | 52.3533 | 2 | 1 | 2 | 1 | 2 | 8 | 3 |

**Table 4** The results of total ranking from proposed models in estimating the response

| | Proposed models | Network result | | | | | | | | | | Total rank score |
|---|---|---|---|---|---|---|---|---|---|---|---|---|
| | | Training dataset | | | | | Testing dataset | | | | | |
| | | $R^2$ | MAE | RMSE | RAE (%) | RRSE (%) | $R^2$ | MAE | RMSE | RAE | RRSE | |
| 1 | MLP | 3 | 1 | 1 | 1 | 1 | 1 | 2 | 1 | 2 | 1 | 14 |
| 2 | M5R | 2 | 3 | 3 | 3 | 3 | 4 | 3 | 4 | 3 | 4 | 32 |
| 3 | DT | 4 | 4 | 4 | 4 | 4 | 3 | 4 | 3 | 4 | 3 | 37 |
| 4 | TM5P | 1 | 2 | 2 | 2 | 2 | 2 | 1 | 2 | 1 | 2 | 17 |

*MLP* Multilayer perceptron, *M5R* M5Rules, *DT* decision table, *TM5P* trees M5P, $R^2$ Correlation coefficient, *MAE* Mean absolute error, *MSE* Root-mean-squared error, *RAE* Relative absolute error, *RRSE* Root relative squared error

can be seen that the lowest training rate is obtained for the MLP model due to its lowest testifying outputs.

A comparison (regarding the results of both training and testing of MLP, M5R, DT, and TM5P datasets) of applied methods is presented in Table 4. In this table, considering the assumption of individual ranks obtained for each model (based on the $R^2$, MAE, RMSE, RAE, and RRSE in Tables 2 and 3), a total ranking is provided. According to this table, the DT (overall score = 37) achieved the supreme accuracy among four models employed in this study (Table 4). After that, M5R and TM5P (total scores of 32 and 17) have shown excellent performance. The notable point in all three tables is the same partial score obtained for all statistical index by each model. Moreover, every model has shown an almost equal accuracy for the training and testing of MLP, M5R, DT, and TM5P datasets. This claim can be proven due to the differences between the values of $R^2$, MAE, RMSE, RAE, and RRSE calculated for each phase. Also, the correlation between the real and modeled values of responses is depicted in Figs. 3 and 4 for the training and testing of MLP, M5R, DT, and TM5P datasets. The best prediction between the data shown on the horizontal (actual responses) and the vertical axis (predicted responses) is demonstrated by the line $x = y$, in the regression chart. According to Figs. 2 and 3, the DT-based solution produced the outputs that are closest to the actual values of responses in both training ($R^2 = 0.9616$) and testing ($R^2 = 0.8964$) phases.

## 5 Summary and conclusions

This study outlines the viability of four machine learning-based models, namely MLP, M5R, DT, and TM5P, in appraising the percentage of drag reduction. The Waikato environment for knowledge analysis (Weka) software was used to train the models. According to prior studies, five key factors influencing the percentage of drag reduction, namely the Reynolds number, polymer concentration, kind of polymer, temperature as well as pipe numbers were considered in this work. To provide the required dataset, the percentage of drag reduction was acquired from the previous researchers' works. In the following, the training (i.e., 80% of the dataset) and testing (i.e., 20% of the dataset) samples were randomly opted to train and validate

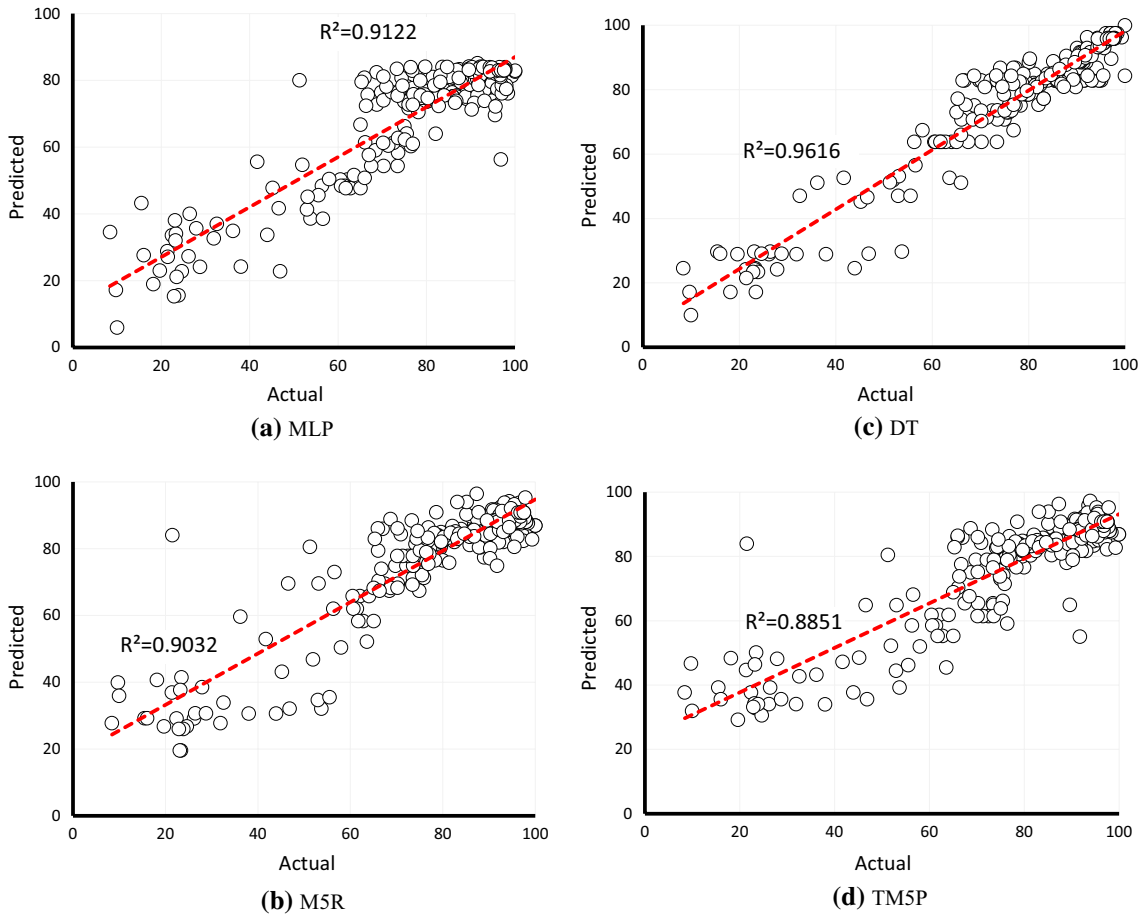


**Fig. 3** The network outputs for the training dataset; **a** MLP, **b** M5R, **c** DT, **d** TM5P

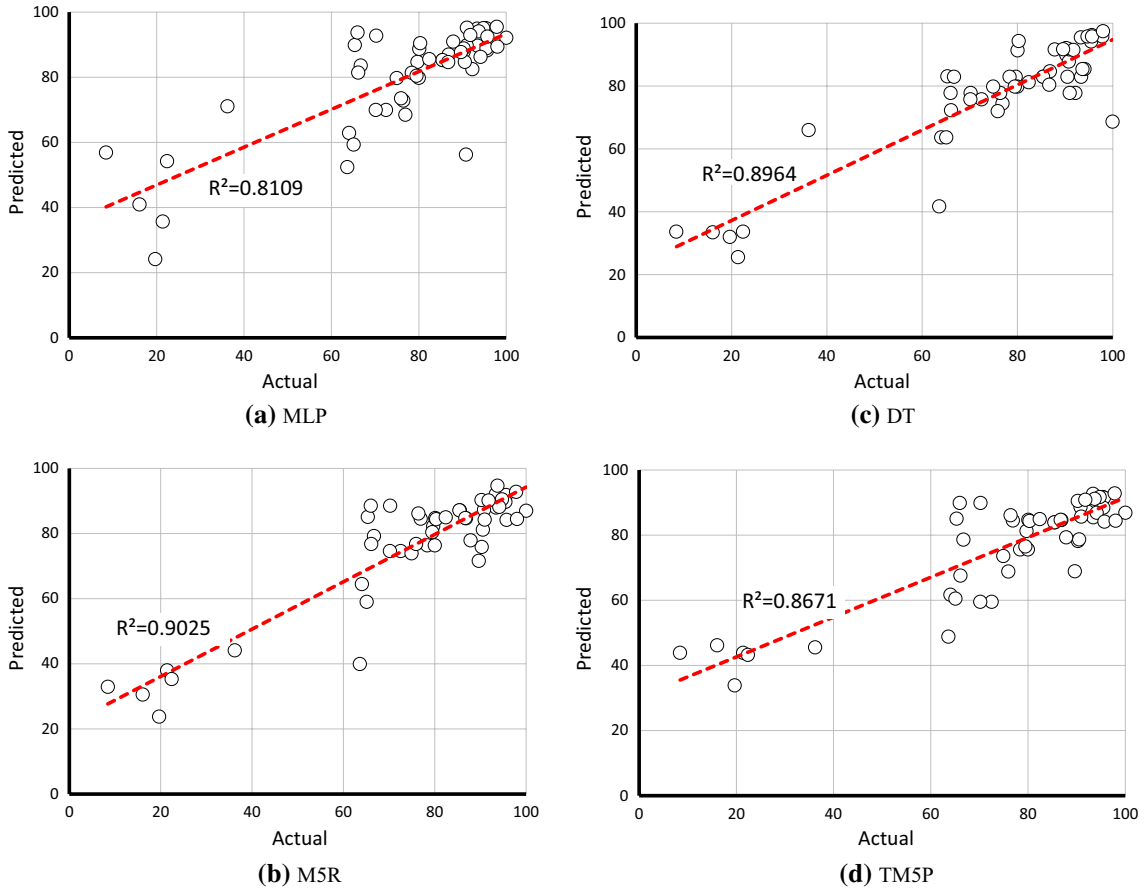


**Fig. 4** The network outputs for the testing dataset; **a** MLP, **b** M5R, **c** DT, **d** TM5P

the performance of the predictive models. To evaluate and compare the proficiency of the MLP, M5R, DT, and TM5P models, a colour intensity model was developed concerning the obtained results of $R^2$, MAE, RMSE, RAE (%), and RRSE (%) indices. Based on the results from different predictive networks, the training and testing $R^2$ for the MLP, M5R, DT, and TM5P models were (0.9122, 0.9032, 0.9616, and 0.8851) and (0.8109, 0.9025, 0.8964, and 0.8671), respectively. The results of total ranking 14, 32, 37, and 17 for the proposed methods of MLP, M5R, DT, and TM5P models indicated the superiority of DT model performance (after analyzing the training and testing stages) in predicting PDR.

## Compliance with ethical standards

**Conflict of interest** The authors declare that they have no conflict of interest.

## References

1. Suzuki H et al (2012) Relaxation behavior of a drag-reducing cationic surfactant solution. Nihon Reoroji Gakkaishi 40(2):85–90
2. Karami HR, Mowla D (2013) A general model for predicting drag reduction in crude oil pipelines. J Pet Sci Eng 111:78–86
3. Pereira AS, Mompean G, Thais L, Soares EJ (2017) Transient aspects of drag reducing plane Couette flows. J Nonnewton Fluid Mech 241:60–69
4. Xi L, Graham MD (2012) Intermittent dynamics of turbulence hibernation in Newtonian and viscoelastic minimal channel flows. J Fluid Mech 693:433–472
5. Kamel A, Shah SN (2009) Effects of salinity and temperature on drag reduction characteristics of polymers in straight circular pipes. J Pet Sci Eng 67(1–2):23–33
6. Li F-C, Kawaguchi Y, Yu B, Wei J-J, Hishida K (2008) Experimental study of drag-reduction mechanism for a dilute surfactant solution flow. Int J Heat Mass Transf 51(3–4):835–843
7. Toms BA (1948) Some observations on the flow of linear polymer solutions through straight tubes at large Reynolds numbers. Proc Int Cong Rheol 135:1948
8. Mysels KJ Flow of thickened fluids. Google Patents 27-Dec-1949

9. Alinovi E, Bottaro A (2018) Apparent slip and drag reduction for the flow over superhydrophobic and lubricant-impregnated surfaces. Phys Rev Fluids 3(12):124002
10. Bhambri P, Narain R, Fleck BA (2016) Thermo-responsive polymers for drag reduction in turbulent Taylor–Couette flow. J Appl Polym Sci 133(46):44191
11. Habibpour M, Clark PE (2017) Drag reduction behavior of hydrolyzed polyacrylamide/xanthan gum mixed polymer solutions. Pet Sci 14(2):412–423
12. Lee J, Zhang Z, Baek S, Kim S, Kim D, Yong K (2016) Bio-inspired dewetted surfaces based on SiC/Si interlocked structures for enhanced-underwater stability and regenerative-drag reduction capability. Sci Rep 6:24653
13. Murai Y, Oiwa H, Takeda Y (2008) Frictional drag reduction in bubbly Couette–Taylor flow. Phys Fluids 20(3):34101
14. Dubief Y, White CM, Terrapon VE, Shaqfeh ESG, Moin P, Lele SK (2004) On the coherent drag-reducing and turbulence-enhancing behaviour of polymers in wall flows. J Fluid Mech 514:271–280
15. Wang X, Chen P, Huang W, Zou J (2018) Development of torque clutch drilling tool and evaluation of drag reduction performance. Adv Mech Eng 10(10):1687814018806655
16. Brostow W, Pal S, Singh RP (2007) A model of flocculation. Mater Lett 61(22):4381–4384
17. Bi C, Zhao Y, Dong G (2015) Numerical study on the hydrodynamic characteristics of biofouled full-scale net cage. China Ocean Eng 29(3):401–414
18. Wang W, Huai W, Zeng Y, Zhou J (2015) Analytical solution of velocity distribution for flow through submerged large deflection flexible vegetation. Appl Math Mech 36(1):107–120
19. Yin L, Zhang H-F, Shi S-Y, Lu Y, Wang Y, Liu X-W (2016) Numerical investigation of relationship between water contact angle and drag reduction ratio of superhydrophobic surfaces. Front Phys 11(3):114701
20. Virk PS (1975) Drag reduction fundamentals. AIChE J 21(4):625–656
21. Sher I, Hetsroni G (2008) A mechanistic model of turbulent drag reduction by additives. Chem Eng Sci 63(7):1771–1778
22. Nisugi K, Hayase T, Shirai A (2004) Fundamental study of aerodynamic drag reduction for vehicle with feedback flow control. JSME Int J Ser B Fluids Therm Eng 47(3):584–592
23. Nesyn GV, Sunagatullin RZ, Shibaev VP, Malkin AY (2018) Drag reduction in transportation of hydrocarbon liquids: from fundamentals to engineering applications. J Pet Sci Eng 161:715–725
24. Karami HR, Mowla D (2012) Investigation of the effects of various parameters on pressure drop reduction in crude oil pipelines by drag reducing agents. J Nonnewton Fluid Mech 177:37–45
25. Mowla D, Naderi A (2006) Experimental study of drag reduction by a polymeric additive in slug two-phase flow of crude oil and air in horizontal pipes. Chem Eng Sci 61(5):1549–1554
26. Pereira AS, Mompean G, Thais L, Thompson RL (2017) Statistics and tensor analysis of polymer coil–stretch mechanism in turbulent drag reducing channel flow. J Fluid Mech 824:135–173
27. Zhao J, Chen P, Liu Y, Zhao W, Mao J (2018) Prediction of field drag reduction by a modified practical pipe diameter model. Chem Eng Technol 41(7):1417–1424
28. Gallego F, Shah SN (2009) Friction pressure correlations for turbulent flow of drag reducing polymer solutions in straight and coiled tubing. J Pet Sci Eng 65(3):147–161
29. Shah SN, Kamel A, Zhou Y (2006) Drag reduction characteristics in straight and coiled tubing—an experimental study. J Pet Sci Eng 53(3–4):179–188
30. Hu L, Hong G, Ma J, Wang X, Chen H (2015) An efficient machine learning approach for diagnosis of paraquat-poisoned patients. Comput Biology Med 59:116-124. https://doi.org/10.1016/j.compbiomed.2015.02.003
31. Yuan C, Moayedi H (2019) Evaluation and comparison of the advanced metaheuristic and conventional machine learning methods for prediction of landslide occurrence. Eng Comput 36:1801–1811
32. Hu L, Hong G, Ma J, Wang X, Chen H (2015) An efficient machine learning approach for diagnosis of paraquat-poisoned patients. Comput Biology Med 59:116–124. https://doi.org/10.1016/j.compbiomed.2015.02.003
33. Chen H-L, Wang G, Ma C, Cai Z-N, Liu W-B, Wang S-J (2016) An efficient hybrid kernel extreme learning machine approach for early diagnosis of Parkinson′ s disease. Neurocomputing 184:131–144. https://doi.org/10.1016/j.neucom.2015.07.138
34. Zhang Y, Liu R, Wang X, Chen H, Li C (2020) Boosted binary Harris hawks optimizer and feature selection. Eng Comput https://doi.org/10.1007/s00366-020-01028-5
35. Chen H, Heidari AA, Chen H, Wang M, Pan Z, Gandomi AH (2020) Multi-population differential evolution-assisted Harris hawks optimization: framework and case studies. Future Generation Comput Syst 111:175–198. https://doi.org/10.1016/j.future.2020.04.008
36. Liu D, Wang S, Huang D, Deng G, Zeng F, Chen H (2016) Medical image classification using spatial adjacent histogram based on adaptive local binary patterns. Comput Biology Med 72:185–200. https://doi.org/10.1016/j.compbiomed.2016.03.010
37. Shen L, Chen H, Yu Z, Kang W, Zhang B, Li H, Yang B, Liu D (2016) Evolving support vector machines using fruit fly optimization for medical data classification. Knowledge-Based Syst 96:61–75. https://doi.org/10.1016/j.knosys.2016.01.002
38. Wang M, Chen H, Yang B, Zhao X, Hu L, Cai Z, Huang H, Tong C (2017) Toward an optimal kernel extreme learning machine using a chaotic moth-flame optimization strategy with applications in medical diagnoses. Neurocomputing 267:69–84. https://doi.org/10.1016/j.neucom.2017.04.060
39. Xia J, Chen H, Li Q, Zhou M, Chen L, Cai Z, Fang Y, Zhou H (2017) Ultrasound-based differentiation of malignant and benign thyroid Nodules: an extreme learning machine approach. Computer methods and programs in biomedicine 147:37–49. https://doi.org/10.1016/j.cmpb.2017.06.005
40. Xu Y, Chen H, Luo J, Zhang Q, Jiao S, Zhang X (2019) Enhanced Moth-flame optimizer with mutation strategy for global optimization. Inf Scis 492:181–203. https://doi.org/10.1016/j.ins.2019.04.022
41. Zhao X, Zhang X, Cai Z, Tian X, Wang X, Huang Y, Chen H, Hu L (2019) Chaos enhanced grey wolf optimization wrapped ELM for diagnosis of paraquat-poisoned patients. Comput Biology Chem 78:481–490. https://doi.org/10.1016/j.compbiolchem.2018.11.017
42. Wang M, Chen H (2020) Chaotic multi-swarm whale optimizer boosted support vector machine for medical diagnosis. Appl Soft Comput J. https://doi.org/10.1016/j.asoc.2019.105946
43. Singh V, Gu N, Wang X (2011) A theoretical framework of a BIM-based multi-disciplinary collaboration platform. Automation in Construction 20:134–144. https://doi.org/10.1016/j.autcon.2010.09.011
44. Zhu J, Wang X, Wang P, Wu Z, Kim MJ (2019) Integration of BIM and GIS: geometry from IFC to shapefile using open-source technology. Automation in Construction 102:105–119. https://doi.org/10.1016/j.autcon.2019.02.014
45. Hauer C, Wagner B, Aigner J, Holzapfel P, Flödl P, Liedermann M, Tritthart M, Sindelar C, Pulg U, Klösch M, Haimann M, Donnum BO, Stickler M, Habersack H (2018) State of the art, shortcomings and future challenges for a sustainable sediment management in hydropower: a review. Renew Sustainable Energy Rev 98:40–55. https://doi.org/10.1016/j.rser.2018.08.031
46. Zhu J, Shi Q, Wu P, Sheng Z, Wang X (2018) Complexity analysis of prefabrication contractors' dynamic price competition in

mega projects with different competition strategies. Complexity 2018:5928235. https://doi.org/10.1155/2018/5928235
47. Chen J, Jiang D, Zhang Y, Zhang P (2020) Emotion recognition from spatiotemporal EEG representations with hybrid convolutional recurrent neural networks via wearable multi-channel headset. Comput Commun 154:58–65. https://doi.org/10.1016/j.comcom.2020.02.051
48. Fu X, Fortino G, Pace P, Aloi G, Li W (2020) Environment-fusion multipath routing protocol for wireless sensor networks. Inform Fusion 53:4–19. https://doi.org/10.1016/j.inffus.2019.06.001
49. Fu X, Pace P, Aloi G, Yang L, Fortino G (2020) Topology optimization against cascading failures on wireless sensor networks using a memetic algorithm. Comput Netw 177:107327. https://doi.org/10.1016/j.comnet.2020.107327
50. Lv Z, Qiao L (2020) Analysis of healthcare big data. Future Generation Comput Syst 109:103–110. https://doi.org/10.1016/j.future.2020.03.039
51. Lv Z, Li X, Lv H, Xiu W (2020) BIM Big Data Storage in WebVRGIS. IEEE Transactions on Industrial Informatics 16:2566–2573. https://doi.org/10.1109/TII.2019.2916689
52. Wang S, Zhang K, van Beek LPH, Tian X, Bogaard TA (2020) Physically-based landslide prediction over a large region: scaling low-resolution hydrological model results for high-resolution slope stability assessment. Environ Modell Software 124:104607. https://doi.org/10.1016/j.envsoft.2019.104607
53. Yang S, Deng B, Wang J, Li H, Lu M, Che Y, Wei X, Loparo KA (2020) Scalable digital neuromorphic architecture for large-scale biophysically meaningful neural network with multi-compartment neurons. IEEE Transactions on Neural Networks and Learning Systems 31:148–162. https://doi.org/10.1109/TNNLS.2019.2899936
54. Hebb DO (1949) Organization of behavior. Wiley, New York
55. ASCE Task Committee on Application of Artificial Neural Networks in Hydrology (2000) Artificial neural networks in hydrology. II: hydrologic applications. J Hydrol Eng 5(2):124–137
56. Wang S-J, Chen H-L, Yan W-J, Chen Y-H, Fu X (2014) Face recognition and micro-expression recognition based on discriminant tensor subspace analysis plus extreme learning machine. Neural Process Lett 39:25–43. https://doi.org/10.1007/s11063-013-9288-7.
57. Xu X, Chen H-L (2014) Adaptive computational chemotaxis based on field in bacterial foraging optimization. Soft Comput 18:797–807. https://doi.org/10.1007/s00500-013-1089-4
58. Moayedi H, Hayati S (2018) Modelling and optimization of ultimate bearing capacity of strip footing near a slope by soft computing methods. Appl Soft Comput 66:208–219
59. Seyedashraf O, Mehrabi M, Akhtari AA (2018) Novel approach for dam break flow modeling using computational intelligence. J Hydrol 559:1028–1038
60. Lv Z, Qiao L (2020) Deep belief network and linear perceptron based cognitive computing for collaborative robots. Applied Soft Computing 92:106300. https://doi.org/10.1016/j.asoc.2020.106300
61. Zhao X, Li D, Yang B, Ma C, Zhu Y, Chen H (2014) Feature selection based on improved ant colony optimization for online detection of foreign fiber in cotton. Appl Soft Comput 24:585–596. https://doi.org/10.1016/j.asoc.2014.07.024
62. Erb RJ (1993) Introduction to backpropagation neural network computation. Pharm Res 10(2):165–170
63. Hu L, Hong G, Ma J, Wang X, Chen H (2015) An efficient machine learning approach for diagnosis of paraquat-poisoned patients. Comput Biol Med 59:116–124. https://doi.org/10.1016/j.compbiomed.2015.02.003
64. Li C, Hou L, Sharma BY, Li H, Chen C, Li Y, Zhao X, Huang H, Cai Z, Chen H (2018) Developing a new intelligent system for the diagnosis of tuberculous pleural effusion. Comput Methods Programs Biomed 153:211–225. https://doi.org/10.1016/j.cmpb.2017.10.022
65. El-Bendary N, Elhariri E, Hazman M, Saleh SM, Hassanien AE (2016) Cultivation-time recommender system based on climatic conditions for newly reclaimed lands in Egypt. Procedia Comput Sci 96:110–119
66. Holmes G, Hall M, Prank E (1999) Generating rule sets from model trees. In: Australasian joint conference on artificial intelligence, pp 1–12
67. Kohavi R (1995) The power of decision tables. In: European conference on machine learning, pp 174–189
68. Chen C, Zhang G, Yang J, Milton JC (2016) An explanatory analysis of driver injury severity in rear-end crashes using a decision table/Naïve Bayes (DTNB) hybrid classifier. Accid Anal Prev 90:95–107
69. Goyal S, Modi N (2017) Data mining using enhanced decision table classifier for online shopping. In: 2017 7th International conference on cloud computing, data science and engineering-confluence, pp 313–318
70. Abbinaya S, Kumar MS (2015) Software effort and risk assessment using decision table trained by neural networks. In: 2015 International conference on communications and signal processing (ICCSP), pp 1389–1394
71. Nguyen TA, Perkins WA, Laffey TJ, Pecora D (1987) Knowledge-base verification. AI Mag 8(2):69–75
72. Quinlan JR (1986) Induction of decision trees. Mach Learn 1(1):81–106
73. Simmonds JA, Gómez JA, Ledezma A (2017) Forecasting sea level changes applying data mining techniques to the Cristobal Bay time series, Panama. J Water Clim Change 8(1):89–101
74. Karami HR, Keyhani M, Mowla D (2016) Experimental analysis of drag reduction in the pipelines with response surface methodology. J Pet Sci Eng 138:104–112
75. Zhao X, Li D, Yang B, Chen H, Yang X, Yu C, Liu S (2015) A two-stage feature selection method with its application. Comput Elect Eng 47:114–125. https://doi.org/10.1016/j.compeleceng.2015.08.011
76. Moayedi H, Aghel B, Foong LK, Bui DT (2019) Feature validity during machine learning paradigms for predicting biodiesel purity. Fuel 26:116498